Journal of Science and Technology in Civil Engineering, HUCE, 2025, 19 (1): 93–107

MECHANICAL BEHAVIOR OF CONCRETE FILLED STEEL TUBULAR COLUMNS WITH HIGH STRENGTH MATERIALS SUBJECTED TO VARIOUS COMPRESSION LOADING SCENARIOS

Hao Dinh Phan[a,*], Tuan Cao Le[a]

[a]*Faculty of Civil Engineering, The University of Danang – University of Science and Technology, 54 Nguyen Luong Bang street, Lien Chieu district, Danang city, Vietnam*

Article history:
Received 28/10/2024, Revised 19/12/2024, Accepted 03/3/2025

Abstract

This study investigates the compressive performance and mechanical behavior of concrete filled steel tubular (CFST) columns constructed with high strength materials under various compression loading scenarios. Thirty specimens, including CFST columns and hollow steel tubes, were evaluated through finite element models (FEMs) in ABAQUS using nonlinear 3D elements to capture the concrete-steel interaction. The materials used had yield strengths (f_y) from 455 to 525 MPa and compressive strengths (f'_c) of 70 to 90 MPa. The CFST columns were subjected to three distinct loading scenarios: compression on the entire column section (CFE), on the concrete core alone (CFC), and on the steel tube alone (CFS). For comparison, hollow steel tubes (EST) were also tested under compressive loads. Results indicated that loading scenarios significantly affected the columns' compressive performance. The highest compressive strength was observed under CFC scenario, followed by CFE, where the steel tube effectively confined the concrete core. CFS scenario produced the lowest strength, similar to EST specimens, where the concrete primarily stabilized the steel tube. Enhanced yield strength (f_y) and compressive strength (f'_c) notably increased CFST compressive strength in both CFC and CFE conditions. The study also found that existing design codes, including EC 4-04, AISC 360-22, and AS/NZS 2327-17, are conservative when predicting the compressive strength of CFST columns using high strength materials.

Keywords: concrete filled steel tubular (CFST) columns; finite element models (FEMs); high strength materials; various compression loading scenarios; confinement effect; current design codes/standards.

https://doi.org/10.31814/stce.huce2025-19(1)-08

1. Introduction

Concrete filled steel tubular (CFST) elements or components have seen growing use in structural applications, such as buildings and bridges, due to the effective synergy between the concrete core and the steel tube, which forms a composite section. This synergy results in enhanced load-bearing capacity, superior compressive strength, improved ductility, and greater overall stability [1]. CFST columns, in particular, are widely utilized in high-rise construction projects, offering significant advantages such as higher strength, excellent ductility, and reduced construction times compared to traditional reinforced concrete (RC) columns. Consequently, CFST columns provide a practical solution to many of the challenges posed by RC columns, such as excessive self-weight, bulky cross-sections, limited ductility, and slower construction timelines.

CFST columns have been extensively studied and adopted in high-rise buildings and long-span bridges, especially in developed countries. As a result, substantial research has focused on the mechanical performance and load-bearing capacity of CFST columns with circular and rectangular/square cross-sections, using a combination of experimental, analytical, and numerical methods

*Corresponding author. *E-mail address:* pdhao@dut.udn.vn (Phan, H. D.)

[2–23]. These studies primarily aim to assess the load-carrying capacity of composite columns, steel tube local buckling, concrete core confinement, and the flexural behavior of CFST beam-columns under diverse loading conditions. While experimental [2, 4, 8, 10–13, 18] and analytical [3, 6, 8–10, 13] approaches have been more common, numerical analyses [5, 7, 12, 14–17, 19–23] have also made significant advancements.

Experimental studies have been conducted to investigate the behavior of CFST columns under different loading conditions and to validate numerical models. Analytical models have also been developed, typically based on idealized assumptions such as perfect bonding between the steel and concrete, uniform material properties, and consistent stress distribution. While these models have offered valuable insights into the behavior of CFST columns, they are limited in their ability to accurately predict performance under more complex or realistic loading scenarios.

Recently, finite element analysis (FEA), supported by advanced software tools, has become increasingly prevalent in studying the behavior of CFST columns. Many researchers have used FEA to investigate the mechanical response of CFST columns under various loading conditions. In the case of axial compression, prior studies have shown that the shape of the cross-section and the steel tube's width-to-thickness (B/t) or diameter-to-thickness (D/t) ratio play a critical role in determining the column's load-bearing capacity [4–7]. Columns with circular cross-sections exhibit better confinement effects than those with non-circular sections. Furthermore, the confinement effect on the concrete core is significantly enhanced under axial compression compared to other loading conditions [8, 13–15, 17, 23].

Various models have been employed in previous studies to simulate the behavior of both the steel tube and the concrete infill in CFST columns [15, 16, 19–21]. Most of these studies have utilized materials with nominal strengths that conform to the limits set by design codes from developed countries, such as EC 4-04, AISC 360-22, and AS/NZS 2327-17 [24–26]. According to these codes, the maximum compressive strength for concrete is 60 MPa, 69 MPa, and 100 MPa, respectively, while the maximum yield strength for structural steel is 460 MPa, 525 MPa, and 690 MPa, respectively. However, some studies have explored the use of materials with strengths that exceed these standard limits. Expanding the application of CFST columns with high strength materials is essential for maximizing the advantages of composite sections and advancing the design of high-rise buildings.

Previous research has developed several useful models for simulating the behavior of CFST columns under axial compressive loads, with a focus on both the steel tube and concrete infill. However, accurately modeling confined concrete, particularly when using high strength materials that exceed the limits specified by EC 4-04 and AISC 360-22 [24, 25], remains a significant challenge. To address the gaps in experimental data for full-scale specimens, a research initiative funded by the authors has focused on numerical studies investigating the mechanical behavior and compressive strength of circular CFST columns with high strength materials. This paper presents the results of these numerical investigations, aiming to analyze the effects of various parameters, such as compressive loading conditions, yield strength of the steel tube, and compressive strength of the concrete core, on the load-bearing capacity of CFST columns, the local buckling of the steel tube, and the confinement effect on the concrete core.

2. Methodology

2.1. Finite element types and meshing technique

A primary objective of this study is to develop finite element models (FEMs) in ABAQUS [27] to simulate the behavior of CFST columns under compressive loads across various loading scenarios. The numerical analysis focuses on the stress and strain distribution within the column, aiming to

provide deeper insights into the mechanical performance of these composite columns. For accurate simulation results that closely mirror real-world behavior, the FEMs must be carefully constructed. The steel tube, concrete core, and loading plates are key interacting components during the loading process, and their behavior must be precisely modeled. In this study, eight-node solid elements (C3D8) in ABAQUS were employed to model both the steel tube and the concrete core, ensuring an accurate representation of the column's structural response.

To ensure the accuracy of the analysis, a mesh convergence study was performed to determine the optimal mesh sizes for both the steel tube and concrete core. For example, a typical mesh size of 40×40 mm was used for both the steel tube and the concrete core, as shown in Fig. 1. The interaction surfaces between the steel tube and concrete core, as well as between these components and the loading plates, were modeled using the interaction and bonding models available in ABAQUS. These models effectively capture the composite action and load transfer mechanisms within the CFST columns. Furthermore, the 'Reference Point' function in ABAQUS was utilized, providing flexibility in applying loading and boundary conditions.

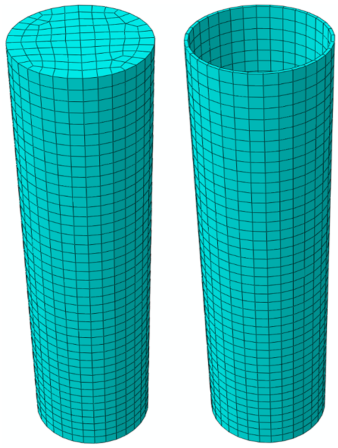

Figure 1. Meshing for concrete core and steel tube components

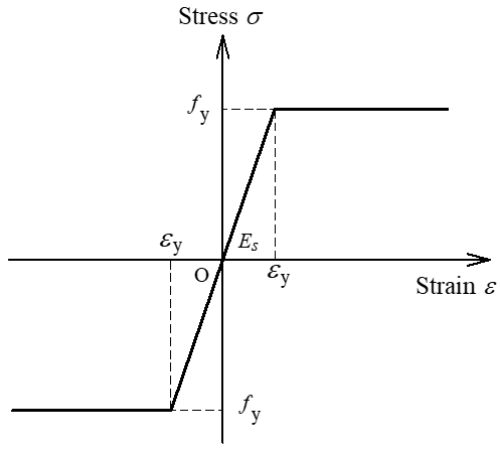

Figure 2. Elasto-plastic model for steel

2.2. *Steel tube and concrete filled models*

In ABAQUS, the elasto-plastic material model, as illustrated in Fig. 2, is used to represent the steel tube component in this study. During the elastic phase, the stress-strain relationship is defined linearly based on the yield strength (f_y) and the modulus of elasticity (E_s) of the steel. Specifically, f_y is taken as the nominal strength of the steel, while E_s is set to 200 GPa, with a Poisson's ratio (ν_s) of 0.3. The steel tubes considered in this analysis have yield strengths of 455 MPa, 490 MPa, and 525 MPa.

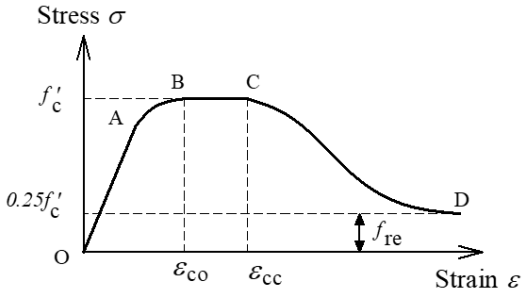

Figure 3. A confined concrete model [23]

In this study, high strength concrete with compressive strengths ranging from 70 to 90 MPa was used. The elastic modulus (E_c) was calculated using the formula proposed in ACI 318-19 [28]. The primary mechanical properties of the concrete material are summarized in Table 1. Developing an accurate and reliable model to simulate the behavior of concrete in CFST columns, particularly for

large-scale specimens, remains a significant challenge in the simulation process. Although various concrete models have been proposed in previous studies for simulating CFST columns under axial compression [29–33], each has limitations in precisely capturing the compressive behavior of these composite structures. To address these limitations, this study adopts the Concrete Damaged Plasticity (CDP) model available in ABAQUS, which incorporates the confinement effect. The confined concrete model, developed by the first author in [23] based on established literature, is proposed for this research. This model aims to more accurately represent the compressive behavior of concrete confined within the steel tube of circular CFST columns. The proposed model is illustrated in Fig. 3.

Table 1. Concrete mechanical factors

Mass density (kg/m^3)	Compressive strength, f'_c (MPa)	Elastic modulus, E_c (MPa)
2400	70	39323
	80	42038
	90	44588

2.3. Steel tube – concrete core interaction modeling

To model the interaction between steel and concrete in CFST columns under axial compressive loading, the *Contact Pair option in ABAQUS was utilized, employing surface-to-surface contact to represent the interaction between the steel tube's inner surface and the concrete core's outer surface. This contact pair method requires the designation of a master surface and a slave surface. To minimize numerical inaccuracies, the slave surface is assigned to the softer material, which in this case is the steel tube, and is usually meshed more finely than the master surface, which corresponds to the concrete core [27]. The contact properties between the surfaces were defined based on their normal and tangential behaviors. The normal behavior was modeled using 'Hard' contact, allowing for separation between surfaces after initial contact. Meanwhile, the tangential behavior was modeled using the 'Coulomb' friction model, with a friction coefficient of 0.2 [17, 23].

2.4. Boundary conditions and loading applying

This study investigated three distinct loading scenarios for CFST column specimens: simultaneous loading of both the steel tube and the concrete core (CFE), loading applied solely to the concrete core (CFC), and loading applied exclusively to the steel tube (CFS). Additionally, empty steel tube (EST) specimens were tested under compressive loading for comparison. The dimensions of the composite and steel column specimens, along with the various loading conditions, are illustrated in Fig. 4. To accurately replicate the real-world behavior of these columns, the boundary conditions and loading configurations were meticulously designed.

For the CFE loading scenario, a 'Discrete Rigid' loading plate type was selected. In contrast, for the CFC, CFS, and EST loading scenarios, the 'Reference Point' (RP) function in ABAQUS was employed to establish boundary conditions and directly apply axial compressive loads to the surface of either the concrete core or the steel tube at the column end. In all these column specimens, boundary conditions and compressive loads were applied at both ends through the RPs. At the bottom end, the column was fully fixed at the first RP, with all six degrees of freedom (DOFs) restricted, while at the top end, it was partially fixed at the second RP, with five DOFs restricted and one DOF released, allowing movement along the column's longitudinal axis. When loading plates were used, the interaction between the concrete core, the steel tube at the column ends, and the loading plates was modeled using the 'Tie' connection available in the ABAQUS library.

In this study, the displacement control method was employed to apply axial compressive forces to the column specimens. Incremental axial displacement was applied at the second RP of each specimen to ensure uniform deformation across the top surface during loading. This technique ensured an even distribution of the axial compressive load at the top end of the column. The RPs for applying the axial compressive loads were positioned at the locations where the concentrated force P was applied, as illustrated in Fig. 4. A displacement loading limit of 35 mm was selected as the optimal value for all column specimens.

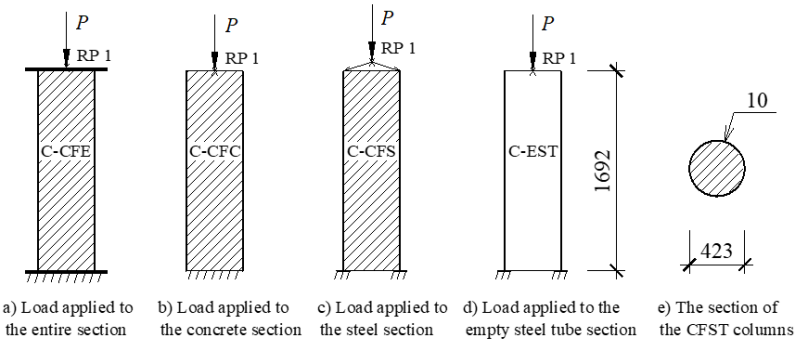

Figure 4. Dimensions of column specimens and applied loading scenarios

2.5. Modeling validation

The FEMs of the various column specimens simulated in this study, utilizing an elasto-plastic model for the steel tube and a confined concrete model [23] for the concrete core, were validated against both experimental and numerical results from previous studies [8, 17], demonstrating good agreement for significant stages. A comparison of the compressive strength (load-carrying capacity) and compression performance between the proposed models and those from prior studies is provided in Table 2 and Fig. 5. During the elastic stage, the axial compression stiffness obtained from the FEM analysis of the column specimens was slightly higher than that derived from experimental testing. This discrepancy can be attributed to the idealized boundary conditions used in the FEM simulations. Furthermore, a significant increase in axial force was observed in Specimen C-CFS during the post-peak stage, as reported in [8] and [17] and shown in Fig. 5(c). This increase was due to the experimental and modeling setup, which included a small air gap between the loading plate and the concrete core surface. This minimal gap caused the loading to be applied simultaneously to both the steel tube and the concrete core. To address this issue, the present study employed a reference point

Table 2. Comparison of compressive strength between proposed models and prior studies [8, 17]

Loading case	P_{Exp} (kN)	P_{Num} (kN)	P_{max} (kN)	P_{max}/P_{Exp}	P_{max}/P_{Num}
C-CFE	2150	2334	2311	1.07	0.99
C-CFC	2220	2914	2621	1.18	0.90
C-CFS	950	994	987	1.04	0.99
C-EST	920	1008	975	1.06	0.97

Notes: P_{Exp} refers to the axial compressive load-carrying capacity of the column under various loading conditions, as determined from the experimental findings of Johansson and Gylltoft [8]. P_{Num} represents the axial compressive load-carrying capacity derived from numerical simulations carried out by Phan and Trinh [17]. P_{max} indicates the axial compressive load-carrying capacity of the column for different loading scenarios, as calculated in the present study.

(RP) for loading, in place of a loading plate. Following validation, these FEMs were used to conduct parametric studies to investigate the effects of various parameters, including loading scenario, steel yield strength (f_y), and concrete compressive strength (f'_c), on the mechanical behavior, compressive strength and deformation capacity of circular CFST columns. The results of these numerical simulations, along with detailed discussions, are presented in the following section.

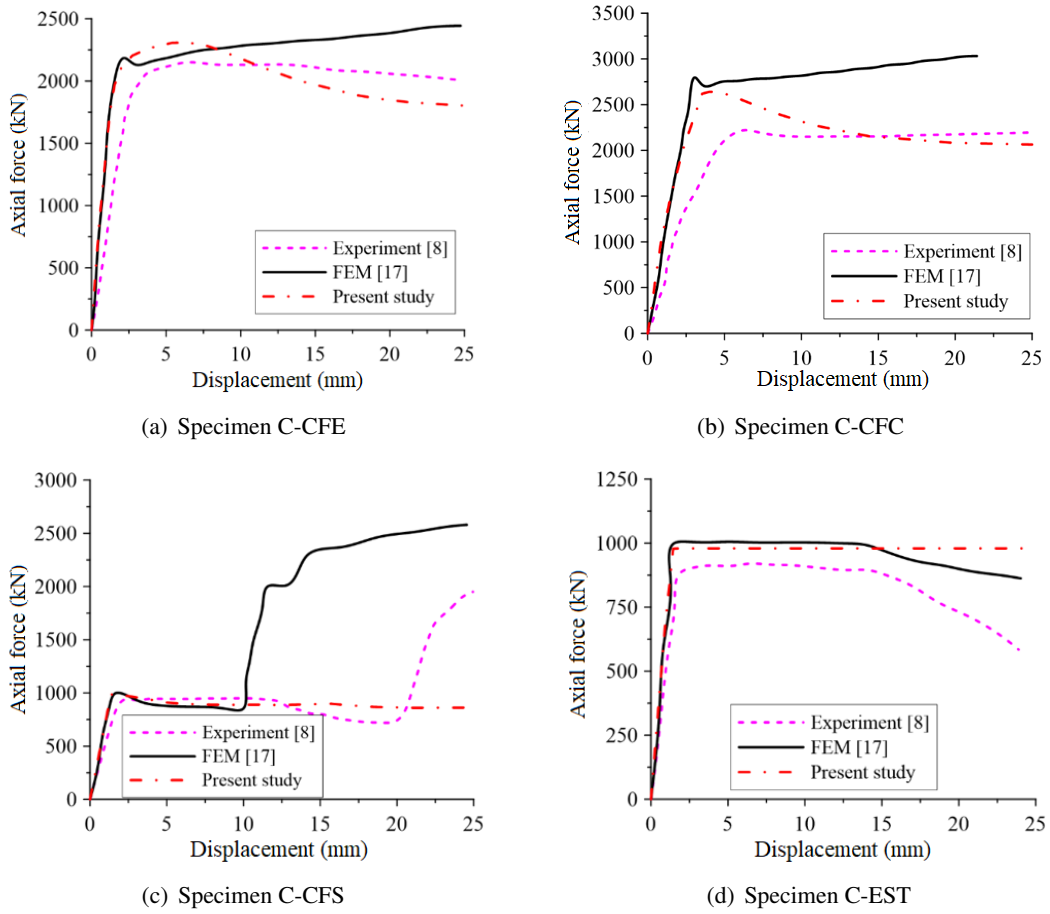

(a) Specimen C-CFE

(b) Specimen C-CFC

(c) Specimen C-CFS

(d) Specimen C-EST

Figure 5. Comparison of compressive behavior between proposed models and prior studies [8, 17]

3. Case studies

3.1. Nominal compressive strengths of CFST columns and loading scenarios

The large-scale circular CFST columns, subjected to axial compressive forces under varying loading conditions, were modeled using ABAQUS. The selected geometric parameters for the CFST columns include an external steel tube diameter (D) of 423 mm, a tube wall thickness (t) of 10 mm, and a column height (H) of 1692 mm (equivalent to 4D), as depicted in Fig. 4.

The nominal compressive strengths of the CFST columns were estimated based on several established design standards, including EC 4-04, AISC 360-22, and AS/NZS 2327-17 [24–26]. These strengths are denoted as $N_{pl,Rd}$ in EC 4-04, P_{no} in AISC 360-22, and N_{us} in AS/NZS 2327-17. Notably, the calculation methods differ across these three standards, as outlined in Eqs. (1) to (3) below.

In EC 4-04, the nominal compressive strength (plastic resistance to compression) $N_{pl,Rd}$ for a circular CFST column cross-section is calculated using Eq. (1).

$$N_{pl,Rd} = A_a f_{yd} + A_c f_{cd} \tag{1}$$

where A_a is cross-sectional area of the structural steel section; f_{yd} is design yield strength of the structural steel; A_c is cross-sectional area of the concrete; f_{cd} is design cylinder compressive strength of the concrete.

In AISC 360-22, the nominal compressive strength P_{no} for a circular CFST column cross-section is calculated as presented in Eq. (2).

$$P_{no} = A_s f_y + 0.95 A_c f_c' \tag{2}$$

where A_s and A_c represent the cross-sectional areas of the steel tube and concrete core, respectively; f_y and f_c' denote the yield strength of the steel and the compressive strength of the concrete. The compressive strength contributed by the steel tube is $P_s = A_s f_y$, while the contribution from the concrete core is $P_c = 0.95 A_c f_c'$.

In AS/NZS 2327-17, the nominal compressive strength N_{us} for a circular CFST column cross-section is calculated as shown in Eq. (3)

$$N_{us} = \varphi k_f A_s \eta_2 f_y + \varphi_c A_c f_c' \left(1 + \frac{\eta_1 t f_y}{d_0 f_c'}\right) \tag{3}$$

where φ is the capacity factor for steel (in compresion $\varphi = 0.9$); A_s is the cross-sectional area of the structural steel section; f_y is the nominal yield strength of the structural steel measured parallel to N_{us}; φ_c is the capacity factor for concrete (in compresion $\varphi_c = 0.65$); A_c is the cross-sectional area of the concrete; f_c' is the characteristic compressive strength of concrete at 28 days; t is the wall thickness of the steel tube; d_0 is the outside diameter of the circular hollow section; η_1, η_2 are coefficients; k_f is the form factor.

As highlighted in the literature, the maximum strength limits for steel and concrete materials vary across the three design standards. EC 4-04 prescribes the lowest upper strength limits, AISC 360-22 offers intermediate limits, and AS/NZS 2327-17 permits the highest material strengths. The strength limits specified by EC 4-04 and AISC 360-22 are generally lower than the material strengths used in this study. This methodology enables a comparison between the predicted load-carrying capacities from these codes and the results obtained from finite element modeling (FEM), providing valuable insights into the behavior of composite columns constructed with high strength materials. The comparison also helps identify potential limitations in the application of EC 4-04 and AISC 360-22 for designing composite structures using high-performance materials, guiding future efforts to extend their applicability.

In this study, concentric compressive loads were applied to column specimens to analyze and evaluate the structural behavior of CFST columns. As outlined in Sub-section 2.4, three distinct loading scenarios were considered for CFST columns (CFE, CFC, and CFS), along with one case for hollow steel tubes (EST). All cases involved compressive forces, with variations applied across three levels for two primary parameters: steel yield strength (455, 490, and 525 MPa) and concrete compressive strength (70, 80, and 90 MPa). Table 3 presents the calculated nominal compressive strengths for circular CFST columns, based on different combinations of steel yield and concrete compressive strengths. Table 4 provides a matrix of the composite columns and steel tubes used in the simulations.

Table 3. Nominal compressive strengths of circular CFST columns by EC 4-04, AISC 360-22, and AS/NZS 2327-17

D (mm)	t (mm)	A_s (mm^2)	f_s (MPa)	A_c (mm^2)	f'_c (MPa)	$N_{pl,Rd}$ (kN)	P_{no} (kN)	N_{us} (kN)
423	10	12 975	455	127 491	70	14 939	14 386	12 886
423	10	12 975	455	127 491	80	16 002	15 598	13 694
423	10	12 975	455	127 491	90	17 065	16 810	14 500
423	10	12 975	490	127 491	70	15 393	14 840	13 420
423	10	12 975	490	127 491	80	16 456	16 052	14 226
423	10	12 975	490	127 491	90	17 519	17 264	15 032
423	10	12 975	525	127 491	70	15 847	15 294	13 945
423	10	12 975	525	127 491	80	16 910	16 506	14 751
423	10	12 975	525	127 491	90	17 973	17 718	15 556
423	10	12 975	455	-	-	5904	5829	5904
423	10	12 975	490	-	-	6358	6271	6322
423	10	12 975	525	-	-	6812	6713	6538

Table 4. Column compressive strength by FEMs and comparison with EC 4-04, AISC 360-22, and AS/NZS 2327-17

Specimen	Load case	f_y (MPa)	f'_c (MPa)	$P_{\max}$ (kN)	$P_{\max}/N_{pl,Rd}$	$P_{\max}/P_{no}$	$P_{\max}/N_{us}$
C-CFE-455-70		455	70	17 817	1.193	1.238	1.383
C-CFE-455-80		455	80	19 254	1.203	1.234	1.406
C-CFE-455-90		455	90	20 266	1.188	1.206	1.398
C-CFE-490-70		490	70	18 306	1.189	1.234	1.364
C-CFE-490-80	CFE	490	80	19 656	1.194	1.225	1.382
C-CFE-490-90		490	90	21 045	1.201	1.219	1.400
C-CFE-525-70		525	70	18 636	1.176	1.219	1.336
C-CFE-525-80		525	80	20 054	1.186	1.215	1.359
C-CFE-525-90		525	90	21 092	1.174	1.190	1.356
C-CFC-455-70		455	70	19 417	1.300	1.350	1.507
C-CFC-455-80		455	80	20 788	1.299	1.333	1.518
C-CFC-455-90		455	90	22 382	1.312	1.332	1.544
C-CFC-490-70		490	70	20 052	1.303	1.351	1.494
C-CFC-490-80	CFC	490	80	21 423	1.302	1.335	1.506
C-CFC-490-90		490	90	22 769	1.300	1.319	1.515
C-CFC-525-70		525	70	20 822	1.314	1.361	1.493
C-CFC-525-80		525	80	22 052	1.304	1.336	1.495
C-CFC-525-90		525	90	23 399	1.302	1.321	1.504
C-CFS-455-70		455	70	5797	0.982	0.995	0.982
C-CFS-455-80		455	80	5797	0.982	0.995	0.982
C-CFS-455-90		455	90	5797	0.982	0.995	0.982
C-CFS-490-70		490	70	6245	0.982	0.996	0.988
C-CFS-490-80	CFS	490	80	6245	0.982	0.996	0.988
C-CFS-490-90		490	90	6245	0.982	0.996	0.988

Specimen	Load case	f_y (MPa)	f'_c (MPa)	$P_{\max}$ (kN)	$P_{\max}/N_{pl,Rd}$	$P_{\max}/P_{no}$	$P_{\max}/N_{us}$
C-CFS-525-70		525	70	6680	0.981	0.995	1.022
C-CFS-525-80		525	80	6680	0.981	0.995	1.022
C-CFS-525-90		525	90	6680	0.981	0.995	1.022
C-EST-455		455	-	5771	0.977	0.990	0.977
C-EST-490	EST	490	-	6205	0.976	0.989	0.981
C-EST-525		525	-	6640	0.975	0.989	1.016

Notes: In the CFE and CFC loading cases, $P_{\max}$ is compared to P_{no} ($N_{pl,Rd}$ or N_{us}). In the CFS and EST loading cases, $P_{\max}$ is compared to P_s (the load-carrying capacity of the steel tube alone).

3.2. FEMs results and compressive strength comparisons

The numerical results, encompassing the compressive strengths (load-carrying capacities) and axial force-displacement relationships for all column specimens, are summarized in Table 4 and illustrated in Figs. 6-8, respectively. Furthermore, typical failure modes and the axial force distribution in both the concrete core and steel tube components for selected columns, are shown in Figs. 9-11 and Fig. 12, respectively. A detailed analysis and discussion of these results are provided in this subsection and the following sub-sections. The load-carrying capacities of all thirty column specimens, labeled as $P_{\max}$ and determined through FEM analysis in this study, are reported in Table 4. In addition, the FEM results under various loading conditions were compared with the predictions from the EC 4-04, AISC 360-22, and AS/NZS 2327-17 standards.

The comparison results in Table 4 clearly show that the CFST column under the CFC loading scenario achieves the highest compressive strength or load-carrying capacity across various levels of f_y and f'_c. Specifically, the compressive strengths obtained from FEMs for the CFST columns exceed those calculated based on EC 4-04, AISC 360-22, and AS/NZS 2327-17 by margins of 29.9% to 31.4%, 31.9% to 36.1%, and 49.3% to 54.4%, respectively. The significantly higher compressive strength in the CFC loading case suggests that applying an axial compressive load directly to the concrete core results in nearly perfect confinement. In comparison, the CFE loading scenario shows compressive strength increases of approximately 17.4% to 20.3%, 19.0% to 23.8%, and 33.6% to 40.6% when compared to the same reference standards. This indicates that when the axial compressive load is applied to the entire composite section of the CFST column, the concrete core remains confined by the steel tube, though with slightly less effectiveness than in the CFC case.

In contrast, for the CFS and EST loading scenarios, the steel tube primarily bears the compressive force, while the concrete core mainly serves to prevent local inward buckling of the steel tube. The comparison data indicate that in the CFS and EST loading scenarios, $P_{\max}$ (FEM) reaches approximately 98.1% to 102.2% and 97.5% to 101.6%, respectively, of the nominal compressive strength of the corresponding steel tubes.

3.3. Axial force – displacement relationships

The diagrams illustrating the relationship between compressive force and axial displacement (P-Δ) for CFST columns and corresponding hollow steel columns, using steel and concrete materials with varying yield and compressive strengths under different loading scenarios, are presented in Figs. 6–8.

The P-Δ curves in Figs. 6–8 demonstrate that across all levels of f_y and f'_c of the constituent materials, the CFE loading scenario exhibits the stiffest compressive behavior in the elastic stage of the composite column, followed by the CFC loading scenario, with the CFS and EST loading

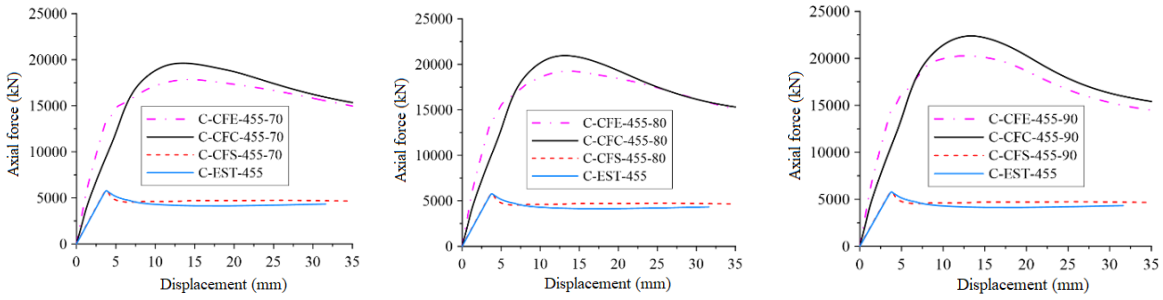

(a) f_c' = 70 MPa (b) f_c' = 80 MPa (c) f_c' = 90 MPa

Figure 6. Axial force – displacement relationship (f_y = 455 MPa)

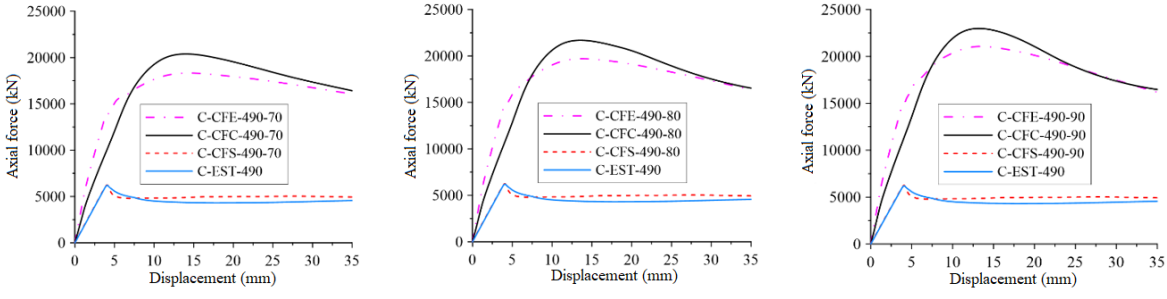

(a) f_c' = 70 MPa (b) f_c' = 80 MPa (c) f_c' = 90 MPa

Figure 7. Axial force – displacement relationship (f_y = 490 MPa)

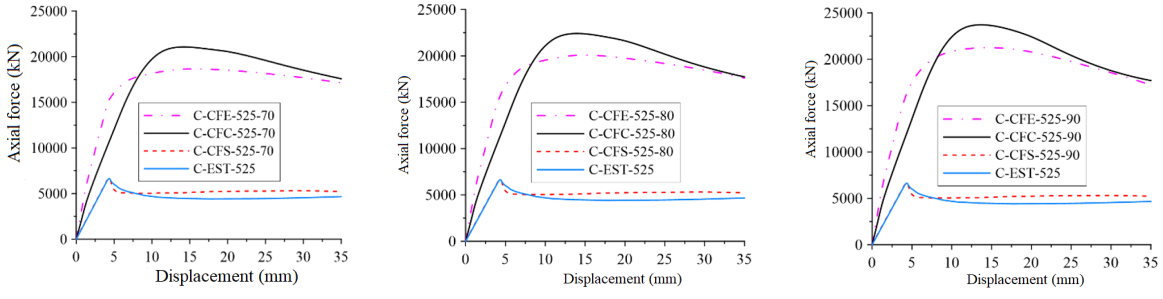

(a) f_c' = 70 MPa (b) f_c' = 80 MPa (c) f_c' = 90 MPa

Figure 8. Axial force – displacement relationship (f_y = 525 MPa)

scenarios displaying the least stiffness. The difference in compressive stiffness between the CFE and CFC loading scenarios is attributed to the load transfer mechanism between the steel tube and the concrete core components.

In the elastic stage, for the CFE loading scenario, both the steel tube and the concrete core simultaneously bear the axial load, resulting in the combined compressive stiffness of the composite column from these two constituent components. In contrast, in the CFC loading scenario, the concrete core initially bears the axial load directly, with the steel tube gradually receiving the load transferred from the concrete core. As a result, the compressive stiffness of the composite column in this stage is primarily influenced by the concrete core.

Conversely, in the post-elastic and strength recovery stages, the stiffness of the composite column

in the CFC loading scenario exceeds that in the CFE loading scenario. This behavior suggests that, in the later stages of compressive loading, the differing mechanical properties of the constituent materials lead to a shift in compressive stiffness. For the CFE loading scenario, the higher Poisson's ratio of the steel compared to that of the concrete may reduce the confinement effect provided by the steel tube on the concrete core, resulting in a decrease in compressive stiffness for the CFST column. In contrast, in the CFC loading scenario, the restrained deformation of the concrete core enhances the confinement effect, leading to the higher compressive stiffness and strength observed in the CFST column during this stage.

The remaining two loading scenarios, CFS and EST, do not exhibit a strength recovery stage. Instead, after reaching the peak value, the compressive strength drops abruptly due to local buckling of the steel tube wall. The results indicate that in the CFS loading scenario, where the steel tube of the CFST column bears the load, the concrete core does not contribute to carrying the axial compressive load; it merely prevents the inward local buckling of the steel tube wall. However, this effect is relatively minor compared to the EST loading scenario.

3.4. Failure modes of column specimens

The failure modes of the column specimens corresponding to the four loading scenarios, with constituent material combinations of f_y = 455 MPa and f_c' = 70 MPa; f_y = 490 MPa and f_c' = 80 MPa; and f_y = 525 MPa and f_c' = 90 MPa, are illustrated in Figs. 9–11. The comparison and failure analysis of these column specimens provide valuable insights into the mechanical behavior of CFST columns and empty steel tube columns when subjected to different compressive loading scenarios using high strength materials.

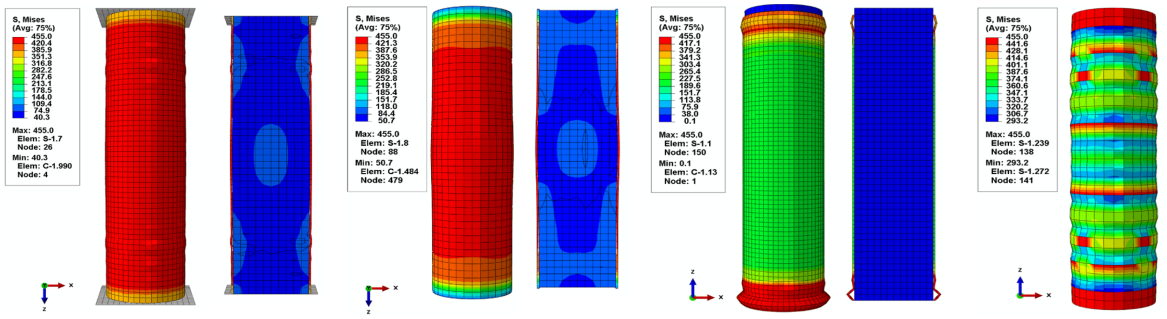

(a) C-CFE-455-70 (b) C-CFC-455-70 (c) C-CFS-455-70 (d) C-EST-455

Figure 9. Failure modes of the columns with f_y = 455 MPa, f_c' = 70 MPa

Based on the deformation and stress distribution images in the steel tube and concrete core, it is evident that different compressive loading scenarios significantly influence the failure modes of the component members and the overall column. For the CFE and CFC loading scenarios, the deformation and stress distribution in the steel tube and concrete core are nearly symmetrical across the cross-section at the column's center. However, a key distinction emerges: in the CFE loading scenario, failure occurs when the steel tube reaches its yield strength (f_y), accompanied by slight local buckling and cracking in the concrete core. In contrast, in the CFC loading scenario, failure is also caused by the steel tube reaching its yield strength (f_y), but with more pronounced cracking in the concrete core. Additionally, the compressive stress in the concrete core for the CFC loading scenario is higher than that in the CFE loading scenario, despite using the same material grades for both the steel tube and concrete core components (Figs. 9(a), (b)–11(a), (b))

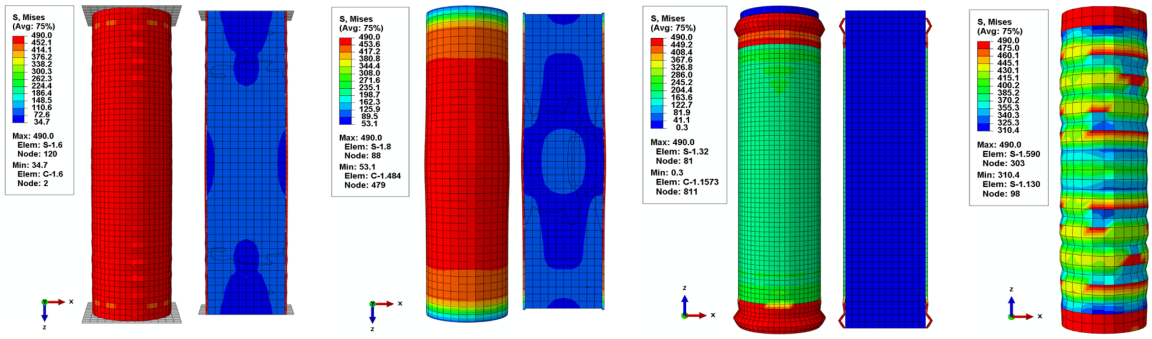

(a) C-CFE-490-80 (b) C-CFC-490-80 (c) C-CFS-490-80 (d) C-EST-490

Figure 10. Failure modes of the columns with f_y = 490 MPa, f'_c = 80 MPa

In the CFS loading scenario, the deformation and stress distribution in the steel tube are ligthly asymmetrical across the cross-section at the column's midpoint, with the concrete core not contributing to the compressive load. In this scenario, the steel tube fails by reaching its yield strength (f_y) and experiences outward local buckling near the top of the column, where axial displacement is applied (Figs. 9(c)–11(c)). Lastly, in the EST loading scenario, Figs. 9(d)–11(d) illustrate that the deformation and stress distribution in the steel tube are symmetrical across the cross-section at the column's center. Failure occurs when the steel tube reaches its yield strength (f_y), accompanied by local buckling that produces both outward and inward (corrugated) deformations.

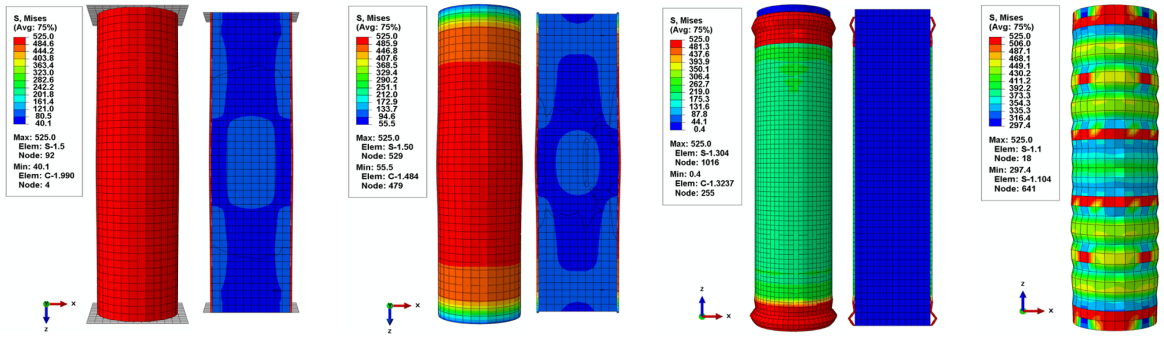

(a) C-CFE-525-90 (b) C-CFC-525-90 (c) C-CFS-525-90 (d) C-EST-525

Figure 11. Failure modes of the columns with f_y = 525 MPa, f'_c = 90 MPa

3.5. Axial force distribution in concrete core and steel tube

Determining the distribution of compressive forces within the concrete core and steel tube enhances the understanding of their combined performance, as well as the confinement effect provided by the outer steel tube on the inner concrete core. This behavior is influenced by the method of load application, particularly the effective interaction between the steel tube and the concrete core, which predominantly occurs in the CFE and CFC loading scenarios. In contrast, for the CFS loading scenario, the analysis results depicted in Figs. 9(c)–11(c) indicate that there is no force transfer between the steel tube and the concrete core. Fig. 12 illustrates the distribution of compressive forces within the structural components of two column specimens, C-CFE-490-90 and C-CFC-490-90, under compressive loading.

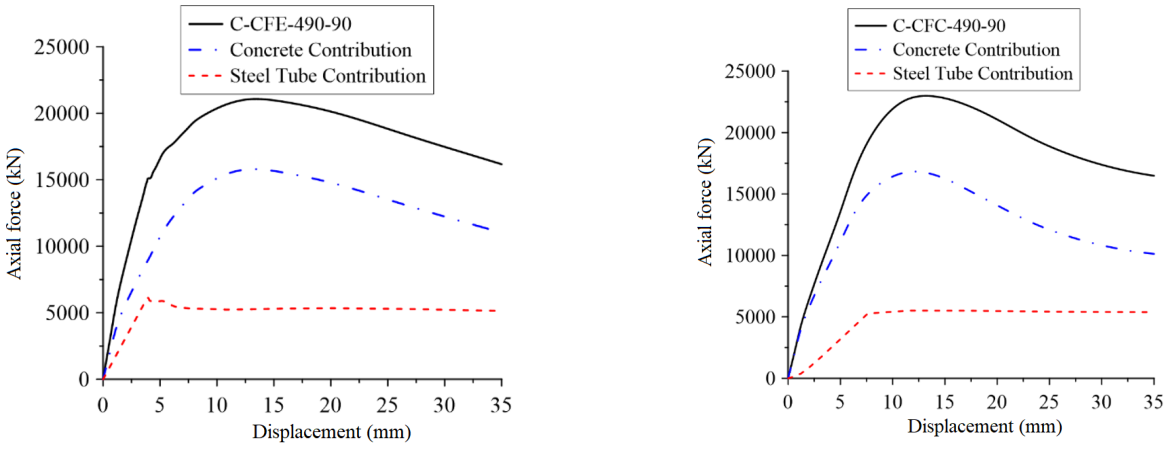

(a) Specimen C-CFE-490-90 (b) Specimen C-CFC-490-90

Figure 12. Axial force distribution in CFST columns

The results in Fig. 12 indicate that the maximum axial compressive force in the concrete core for both the CFE and CFC loading scenarios surpasses the compressive strength of the concrete core as predicted by EC 4-04, AISC 360-22, and AS/NZS 2327-17 [24–26]. This increase in compressive strength, relative to the design code predictions, is attributed to the confinement effect provided by the steel tube surrounding the concrete core. Specifically, the column specimen C-CFE-490-90 exhibits increases of 41.4%, 44.8%, and 69.6%, while C-CFC-490-90 shows increases of 50.6%, 54.1%, and 80.5%, respectively. These results highlight that CFST columns under the CFC loading scenario demonstrate the most effective confinement.

4. Conclusions

Based on the numerical simulation results in this study, the following conclusions can be drawn:

The compressive strength and mechanical behavior of circular CFST columns are influenced by the method of compressive load application. Among the loading scenarios, the CFC scenario yields the highest compressive strength, followed by the CFE scenario. In contrast, the CFS scenario results in only a slight increase in compressive strength compared to the empty steel tube column (EST).

The P-Δ curves remain consistent across all loading scenarios as f_y and f_c' increase at various levels. In the linear elastic stage, CFST columns in the CFE loading scenario display stiffer compressive behavior than those in the CFC loading scenario; however, this trend reverses beyond the linear elastic stage. The P-Δ curves for the CFS and EST loading scenarios are almost identical.

Increasing f_y and f_c' at various levels significantly enhances the compressive strength of CFST columns in both CFE and CFC loading scenarios. However, the failure modes exhibit only slight variations across the scenarios. In the CFE group, columns fail when the steel tube reaches its yield strength and experiences local buckling, often accompanied by cracking in the concrete core. Similarly, in the CFC group, failure occurs when the steel tube reaches yield strength, followed by potential cracking of the concrete core. In contrast, failure in the CFS and EST groups is primarily due to the steel tube reaching yield strength and undergoing local buckling.

The confinement effect provided by the steel tube greatly enhances the compressive strength of the concrete core in the CFC and CFE loading scenarios, with the most significant confinement observed in the CFC loading scenario, where the concrete core is subjected to nearly three-dimensional compression. Meanwhile, this confinement effect is absent in the CFS loading scenario.

The simulation results indicate that AS/NZS 2327-17 provides the most conservative design approach for CFST columns utilizing high strength materials. Additionally, the findings demonstrate that both EC 4-04 and AISC 360-22 offer reliable predictions for the compressive strength of these composite columns, with EC 4-04 showing the closest alignment to the simulation results obtained in this study.

Acknowledgments

The authors would like to express their sincere gratitude to The University of Danang – University of Science and Technology, Vietnam, for their financial support of the research project titled "Analysis of Mechanical Behavior and Compressive Strength of Concrete Filled Steel Tubular Columns" (Project Code: T2024-02-09).

References

[1] Uy, B. (1998). Concrete-filled fabricated steel box columns for multi-storey buildings: behaviour and design. *Progress in Structural Engineering and Materials*, 1(2):150–158.

[2] Ge, H., Usami, T. (1992). Strength of concrete-filled thin-walled steel box columns: experiment. *Journal of Structural Engineering*, 118(11):3036–3054.

[3] Ge, H., Usami, T. (1994). Strength analysis of concrete-filled thin-walled steel box columns. *Journal of Constructional Steel Research*, 30(3):259–281.

[4] Schneider, S. P. (1998). Axially loaded concrete-filled steel tubes. *Journal of Structural Engineering*, 124 (10):1125–1138.

[5] Shams, M., Saadeghvaziri, M. (1999). Nonlinear response of concrete-filled steel tubular columns under axial loading. *ACI Structural Journal*, 96(6):1009–1017.

[6] Susantha, K. A. S., Ge, H., Usami, T. (2001). Uniaxial stress–strain relationship of concrete confined by various shaped steel tubes. *Engineering Structures*, 23(10):1331–1347.

[7] Hu, H.-T., Huang, C.-S., Wu, M.-H., Wu, Y.-M. (2003). Nonlinear analysis of axially loaded concrete-filled tube columns with confinement effect. *Journal of Structural Engineering*, 129(10):1322–1329.

[8] Johansson, M., Gylltoft, K. (2002). Mechanical Behavior of Circular Steel-Concrete Composite Stub Columns. *Journal of Structural Engineering*, 128(8):1073–1081.

[9] Fujimoto, T., Mukai, A., Nishiyama, I., Sakino, K. (2004). Behavior of Eccentrically Loaded Concrete-Filled Steel Tubular Columns. *Journal of Structural Engineering*, 130(2):203–212.

[10] Han, L.-H. (2004). Flexural behaviour of concrete-filled steel tubes. *Journal of Constructional Steel Research*, 60:313–337.

[11] Yu, Z., Ding, F., Cai, C. S. (2007). Experimental behavior of circular concrete-filled steel tube stub columns. *Journal of Constructional Steel Research*, 63:165–174.

[12] Han, L.-H., Liu, W., Yang, Y.-F. (2008). Behaviour of concrete-filled steel tubular stub columns subjected to axially local compression. *Journal of Constructional Steel Research*, 64:377–387.

[13] Liu, J., Zhou, X. (2010). Behavior and strength of tubed RC stub columns under axial compression. *Journal of Constructional Steel Research*, 66(1):28–36.

[14] Yu, Q., Tao, Z., Liu, W., Chen, Z.-B. (2010). Analysis and calculations of steel tube confined concrete (STCC) stub columns. *Journal of Constructional Steel Research*, 66(1):53–64.

[15] Tao, Z., Wang, Z.-B., Yu, Q. (2013). Finite element modelling of concrete-filled steel stub columns under axial compression. *Journal of Constructional Steel Research*, 89:121–131.

[16] Thai, H.-T., Uy, B., Khan, M., Tao, Z., Mashiri, F. (2014). Numerical modelling of concrete-filled steel box columns incorporating high strength materials. *Journal of Constructional Steel Research*, 102:256–265.

[17] Phan, H. D., Trinh, H. H. (2017). Analysis of mechanical behaviour of circular concrete filled steel tube columns using high strength concrete. In *Mechanics of Structures and Materials: Advancements and Challenges*, 231–236.

[18] Phan, H. D., Lin, K. C. (2020). Seismic behavior of full-scale square concrete filled steel tubular columns under high and varied axial compressions. *Earthquakes and Structures*, 18:677–689.

[19] Phan, H. D. (2021). Numerical analysis of seismic behavior of square concrete filled steel tubular columns. *Journal of Science and Technology in Civil Engineering - NUCE*, 15(2):127–140.

[20] Thai, S., Cuong, N. H., Thuat, D. V. (2021). Finite element modelling of rectangular concrete-filled steel tube stube columns incorporating high strength and ultra-high strength materials under concentric axial compression. *Journal of Science and Technology in Civil Engineering - HUCE (NUCE)*, 15(4):74–87.

[21] Phan, H. D., Lin, K. C., Phan, H. T. (2022). Numerical simulation of full-scale square concrete filled steel tubular (CFST) columns under seismic loading. In *Modern Mechanics and Applications: Select Proceedings of ICOMMA 2020*, Springer Singapore, 875–889.

[22] Phan, H. D., Lin, K. C. (2022). Seismic Performance of Concrete Filled Steel Tubular (CFST) Columns with Variously Axial Compressive Loads. In *Modern Mechanics and Applications: Select Proceedings of ICOMMA 2020*, Springer Singapore, 915–925.

[23] Phan, H. D., Dao, L. K. T. (2023). Numerical analysis of compressive behavior of circular concrete filled steel tubular columns with high to ultra-high strength materials. *Journal of Science and Technology in Civil Engineering (JSTCE) - HUCE*, 17(2):83–98.

[24] EN 1994-1-1:2004 (2004). *Eurocode 4: Design of composite steel and concrete structures - Part 1-1: General rules and rules for buildings*. European Committee for Standardization, Brussels, Belgium.

[25] ANSI/AISC 360-22 (2022). *Specification for Structural Steel Building*. American Institute of Steel Construction, Chicago, Illinois, USA.

[26] AS/NZS 2327:2017 (2017). *Composite structures – Composite steel-concrete construction in buildings*. Standards Australia/Standards New Zealand, Sydney/Wellington, Australia/New Zealand.

[27] SIMULIA (2016). *Abaqus Analysis User's and Abaqus/CAE User's Guides*.

[28] ACI 318-19 (2019). *Building Code Requirements for Structural Concrete*. American Concrete Institute, Farmington Hills, Michigan, USA.

[29] Tasdemir, M. A., Tasdemiry, C., Akyuz, S., Jefferson, A. D., Lydon, F. D., Barr, B. I. G. (1998). Evaluation of Strains at Peak Stresses in Concrete: A Three-Phase Composite Model Approach. *Cement and Concrete Research*, 20:301–318.

[30] Binici, B. (2005). An Analytical Model for Stress–Strain Behavior of Confined Concrete. *Engineering Structures*, 27(7):1040–1051.

[31] Xiao, Q. G., Teng, J. G., Yu, T. (2010). Behavior and Modeling of Confined High-Strength Concrete. *Journal of Composites for Construction*, 14:249–259.

[32] Samani, A. K., Attard, M. M. (2012). A Stress–Strain Model for Uniaxial and Confined Concrete Under Compression. *Engineering Structures*, 41:335–349.

[33] Tao, Z., Wang, Z.-B., Yu, Q. (2013). Finite Element Modelling of Concrete-Filled Steel Stub Columns Under Axial Compression. *Journal of Constructional Steel Research*, 89:121–131.